Pionic enhancement in quasielastic $(\vec{p},\vec{n})$ reactions at 345 MeV

T. Wakasa,[1,*] H. Sakai,[2,3] M. Ichimura,[4] K. Hatanaka,[5] M. B. Greenfield,[6] M. Hatano,[2] J. Kamiya,[7] H. Kato,[2] K. Kawahigashi,[8] Y. Maeda,[2] Y. Nakaoka,[2] H. Okamura,[9] T. Ohnishi,[3] H. Otsu,[10] K. Sekiguchi,[3] K. Suda,[11] A. Tamii,[5] T. Uesaka,[12] T. Yagita,[1] and K. Yako[2]

[1]*Department of Physics, Kyushu University, Higashi, Fukuoka 812-8581, Japan*
[2]*Department of Physics, The University of Tokyo, Bunkyo, Tokyo 113-0033, Japan*
[3]*The Institute of Physical and Chemical Research, Wako, Saitama 351-0198, Japan*
[4]*Faculty of Computer and Information Sciences, Hosei University, Koganei, Tokyo 184-8584, Japan*
[5]*Research Center for Nuclear Physics, Osaka University, Ibaraki, Osaka 567-0047, Japan*
[6]*Division of Natural Science, International Christian University, Mitaka, Tokyo 181-8585, Japan*
[7]*Accelerator Group, Japan Atomic Energy Research Institute, Tokai, Ibaraki 319-1195, Japan*
[8]*Department of Information Sciences, Kanagawa University, Hiratsuka, Kanagawa 259-1293, Japan*
[9]*Cyclotron and Radioisotope Center, Tohoku University, Sendai, Miyagi 980-8578, Japan*
[10]*Department of Physics, Tohoku University, Sendai, Miyagi 980-8578, Japan*
[11]*Department of Physics, Saitama University, Saitama, Saitama 338-8570, Japan*
[12]*Center for Nuclear Study, The University of Tokyo, Bunkyo, Tokyo 113-0033, Japan*

(Received 14 January 2004; published 25 May 2004)

Differential cross sections and a complete set of polarization observables have been measured for quasielastic $(\vec{p},\vec{n})$ reactions on ^{12}C and ^{40}Ca at a bombarding energy of 345 MeV. The laboratory momentum transfers are $q_{\rm lab} \simeq 1.2$, 1.7, and 2.0 fm^{-1} for ^{12}C and $q_{\rm lab} \simeq 1.7$ fm^{-1} for ^{40}Ca. In these momentum transfer regions, the isovector spin-longitudinal interaction is attractive where the one-pion exchange is dominant. The spin-longitudinal and spin-transverse polarized cross sections, ID_q and ID_p, are deduced. The theoretically expected enhancement in the spin-longitudinal mode is observed at $q_{\rm lab} \simeq 1.7$ and 2.0 fm^{-1}. The observed ID_q is consistent with the pionic enhanced ID_q evaluated in distorted wave impulse approximation (DWIA) calculations employing random phase approximation (RPA) response functions. The enhanced ID_q implies the existence of a precursor to pion condensation in nuclei. On the other hand, the theoretically predicted quenching in the spin-transverse mode is not observed. The observed ID_p is not quenched, but rather enhanced relative to that predicted via the DWIA+RPA calculations. Two-step contributions are responsible in part for the enhancement of ID_p.

DOI: 10.1103/PhysRevC.69.054609 PACS number(s): 25.40.Kv, 24.70.+s

I. INTRODUCTION

The nuclear collectivity in spin-isospin modes has been of considerable concern in nuclear physics. At fairly large momentum transfer, $q > 1$ fm^{-1}, Alberico *et al.* [1] made a very interesting prediction for the quasielastic region, based on the random phase approximation (RPA) including the Δ isobar degrees of freedom. They claimed that the spin-longitudinal response function $R_L(q,\omega)$ should be enhanced and soften (shift toward lower energy transfer) with respect to the free response function, where ω is the energy transfer. On the contrary, the spin-transverse response function $R_T(q,\omega)$ should be quenched and hardened (shift toward higher energy transfer) in the same region. The enhancement of R_L is attributed to the collectivity induced by the attraction of the one-pion exchange interaction, and has aroused much interest in connection with both the precursor phenomena of the pion condensation [1–5] and the pion excess in the nucleus [6–11]. The Δ isobar plays a crucial role for this collectivity [12]. The quenching of R_T, on the other hand, is induced by the repulsion of the spin-transverse interaction generated by the short-range correlation and the exchange effects in balance with the one rho-meson exchange attraction.

The R_T values of the quasielastic electron scattering have been reported by the Saclay [13–15] and Bates [16–19] groups. The electron scattering is a good probe for the study of R_T because the electron can survey the entire nuclear volume with little distortion. However, in a one-photon exchange plane wave Born approximation (PWBA), it cannot examine the spin-longitudinal response R_L.

The $(\vec{p},\vec{p})$ and $(\vec{p},\vec{n})$ reactions can investigate both R_L and R_T, and a measurement of a complete set of polarization transfer coefficients D_{ij} allows us to extract them within a framework of a plane wave impulse approximation (PWIA) with eikonal and optimal factorization approximations [20–23]. Carey *et al.* [24], and later Rees *et al.* [25], reported a complete set of D_{ij} for the quasielastic $(\vec{p},\vec{p}')$ scattering on ^{2}H, Ca, and Pb at an incident beam energy of $T_p = 500$ MeV. Many other measurements [26–28] of a complete set of D_{ij} have been also performed for quasielastic $(\vec{p},\vec{p}')$ scattering at momentum transfer $q_{\rm lab}$ near the expected maximum of the attractive spin-longitudinal interaction ($q_{\rm lab} \simeq 1.7$ fm^{-1}). Surprisingly, the experimentally ex-

*Electronic address: wakasa@phys.kyushu-u.ac.jp; http://www.kutl.kyushu-u.ac.jp/~member/wakasa

tracted R_L/R_T ratios are less than or equal to unity, which contradicts the theoretical predictions of the enhanced R_L and the quenched R_T. However, certain aspects of the estimation of these ratios are questionable because (a) the (p,p') scattering mixes the isoscalar and isovector contributions [24,25,29,30] and (b) the method of reaction analysis does not treat the nuclear distortions, especially the spin-dependent distortions properly. Ichimura *et al.* [30] first made a distorted wave impulse approximation (DWIA) calculation in a primitive stage.

Measurements of a complete set of D_{ij} for quasielastic $(\vec{p},\vec{n})$ reactions on ^{2}H, ^{12}C, and ^{40}Ca at $T_p=494$ MeV and $\theta_{\rm lab}=12.5°$, 18°, and 27° were performed at Los Alamos Meson Physics Facility (LAMPF) [31–33]. Measurements at $T_p=346$ MeV and $\theta_{\rm lab}=22°$ were carried out later at the Research Center for Nuclear Physics (RCNP) for ^{2}H, ^{6}Li, ^{12}C, ^{40}Ca, and ^{208}Pb targets [34]. Hautala *et al.* [35] also reported on a complete set of D_{ij} for ^{12}C, ^{40}Ca, and ^{208}Pb targets at $T_p=197$ MeV and $\theta_{\rm lab}=13°$, 24°, 37°, and 48° measured at Indiana University Cyclotron Facility (IUCF). These experiments focused exclusively on the isovector contribution. The ratios R_L/R_T of pure isovector spin response functions obtained from these measurements were also less than or equal to unity. From these results, it has often been concluded that there is no enhancement in R_L, i.e., no collective enhancement of the pionic modes [36,37]. Koltun [11] analyzed the data with help of sum rules and claimed that there is no collective enhancement of the pionic modes in contradiction to the prediction of the RPA calculations.

However, before reaching such a conclusion, other questions, such as the validity of PWIA with the eikonal approximation, etc., should be answered. The experimental evaluation of spin response functions is based on PWIA with an effective nucleon number approximation for distortion effects [23]. In these approximations, the spin-longitudinal, ID_q, and spin-transverse, ID_p, polarized cross sections are proportional to R_L and R_T, respectively. Recently, Kawahigashi *et al.* [38] elaborated DWIA calculations employing the RPA response functions designated herein as DWIA+RPA. They showed that the proportionality between ID_q and R_L and between ID_p and R_T does not hold well. They also showed that ID_q for ^{12}C, ^{40}Ca$(\vec{p},\vec{n})$ reactions at $T_p=494$ and 346 MeV and at $q_{\rm lab}\simeq 1.7$ fm^{-1} were reasonably well reproduce by the DWIA+RPA calculations. This result is consistent with the predicted pionic enhancement in R_L. However, the ID_p are significantly underestimated in their calculations. They concluded that the relatively large excess of experimental versus theoretical ID_p values is responsible for the anomalous R_L/R_T ratio. Excessive spin-transverse mode in the $(\vec{p},\vec{n})$ reaction relative to that obtained via the quasielastic electron scattering has been noted [32–34].

In this paper, we present the measurements of a complete set of D_{ij} for the quasielastic $(\vec{p},\vec{n})$ reaction on ^{12}C at $T_p=345$ MeV and $\theta_{\rm lab}=16°$, 22°, and 27°, which correspond to $q_{\rm lab}=1.2$, 1.7, and 2.0 fm^{-1} at the quasielastic peak. These momentum transfers cover the region of the LAMPF measurement at $T_p=494$ MeV. However, the free *NN t*-matrix elements are significantly different from those at $T_p=494$ MeV. Furthermore, the distortion in the nuclear mean field is minimal for a nucleon kinetic energy of about 300 MeV.

The differential cross sections and a complete set of polarization observables are used to separate the former into nonspin (ID_0), spin-longitudinal (ID_q), and two spin-transverse (ID_n and ID_p) polarized cross sections (see Sec. IV). The spin-longitudinal and spin-transverse polarized cross sections, ID_q and ID_p, respectively, are compared with those calculated in DWIA+RPA in order to assess nuclear correlation effects. The theoretical calculations reproduce ID_q reasonably well below the quasielastic peak, whereas they somewhat underestimate the data beyond the quasielastic peak. For ID_p, the calculations significantly underestimate the data over the entire region. Calculations including two-step contributions account for the underestimation of the spin-longitudinal cross section ID_q beyond the quasielastic peak, and they partly account for the underprediction of the spin-transverse cross section ID_p in the DWIA+RPA calculations.

II. EXPERIMENTAL METHODS

The experiment was performed at the Neutron Time-Of-Flight (NTOF) facility [39] at the RCNP, Osaka University using the neutron detector/polarimeter NPOL2 [39–41]. Detailed descriptions of the NTOF facility and the NPOL2 system are found in Refs. [39–41]. The description of the present experimental setup is presented in the previous paper [42]. Therefore we only describe the targets.

A natural carbon target (98.9% ^{12}C) with a thickness of 172 mg/cm^2 was used for the measurement of cross sections and analyzing powers, whereas a target of 682 mg/cm^2 was used for the measurement of D_{ij} in order to achieve reasonable statistical accuracy. Typical beam currents were 10 and 50 nA for the cross section and D_{ij} measurements, respectively. We also used ^{7}Li and CD_2 targets for normalization of the cross sections and calibration of the effective analyzing powers of NPOL2, respectively.

III. RESULTS

The sideways *S*, normal *N*, and longitudinal *L* coordinates are used to describe the polarization observables. They are defined by the proton and neutron momenta, $\hat{\mathbf{k}}_{\rm lab}$ and $\hat{\mathbf{k}}'_{\rm lab}$, in the laboratory frame as $\hat{\mathbf{L}}=\hat{\mathbf{k}}_{\rm lab}$, $\hat{\mathbf{L}}'=\hat{\mathbf{k}}'_{\rm lab}$, $\hat{\mathbf{N}}=\hat{\mathbf{N}}'=(\mathbf{k}_{\rm lab}\times\mathbf{k}'_{\rm lab})/|\mathbf{k}_{\rm lab}\times\mathbf{k}'_{\rm lab}|$, $\hat{\mathbf{S}}=\hat{\mathbf{N}}\times\hat{\mathbf{L}}$, and $\hat{\mathbf{S}}'=\hat{\mathbf{N}}'\times\hat{\mathbf{L}}'$.

The double differential cross sections as a function of energy transfer $\omega_{\rm lab}$ in the laboratory frame are shown in Fig. 1 for the ^{12}C$(\vec{p},\vec{n})$ reaction at $T_p=345$ MeV and $\theta_{\rm lab}=16°$, 22°, and 27°. In addition to the statistical uncertainty, there is about 2% uncertainty in the determination of the integrated beam current. The systematic uncertainty in the cross section also includes the uncertainties both of the ^{7}Li cross section (3%) and of the thickness of the ^{12}C target (3%).

The present differential cross sections were found to be systematically smaller than our previous data [34]. The difference is most likely due to the beam loss caused by the

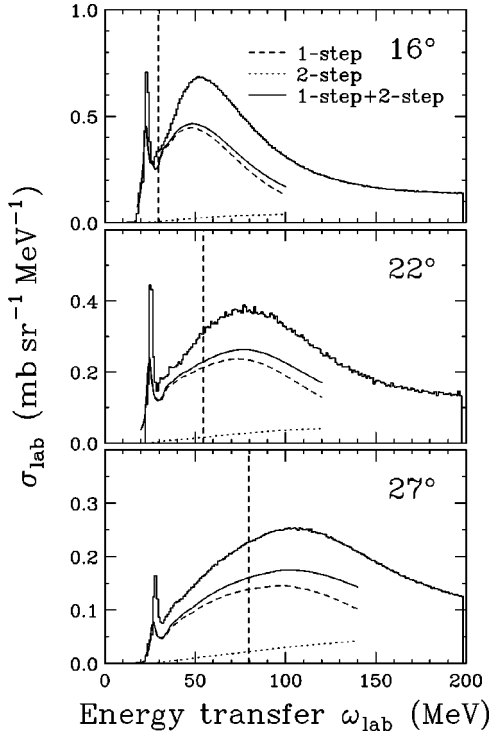

FIG. 1. Cross section spectra for the ^{12}C(p,n) reaction at T_p = 345 MeV and $\theta_{\rm lab}$ = 16°, 22°, and 27°. The data are binned in 1 MeV steps. The dashed and dotted curves correspond to the theoretical predictions for the contributions from one- and two-step processes, respectively. The solid curves are the sums of these contributions. The vertical dashed lines mark the energy transfer for the free *np* scattering.

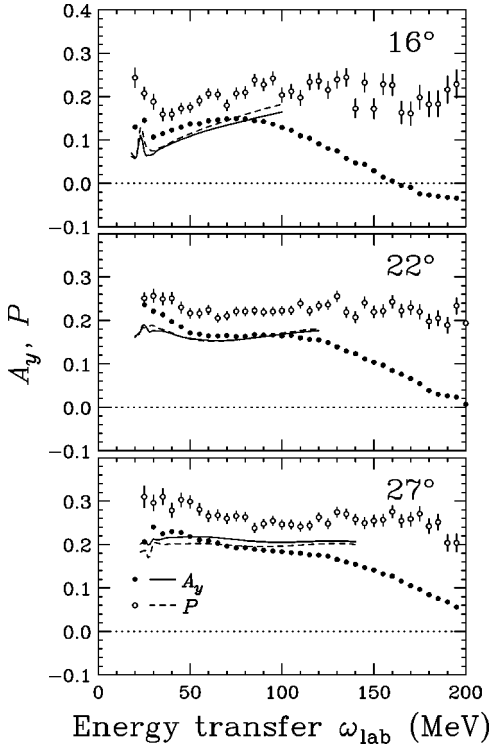

FIG. 2. Analyzing powers A_y and induced polarizations P for the ^{12}C(p,n) reaction at T_p = 345 MeV and $\theta_{\rm lab}$ = 16°, 22°, and 27°. The data are binned in 5 MeV steps. The solid and dashed curves represent the DWIA + RPA calculations for analyzing powers and induced polarizations, respectively.

multiple scattering effects in the previously used thicker targets, as discussed in Ref. [42].

The main feature of the cross section is the broad bump due to the quasielastic process. The energy transfers for the free *np* scattering are represented with vertical dotted lines. The observed peaks of the quasielastic spectra are more than 20 MeV higher than those for the free *np* scattering. The solid curves are the results of the DWIA calculations with the one- and two-step processes. The DWIA calculations reproduce the experimental differential cross sections in shape, but they are much smaller in magnitude around the quasielastic peak. This discrepancy comes from the quenching of the spin-transverse mode, which will be discussed in Secs. V and VI.

Figure 2 shows the analyzing powers A_y and the induced polarizations P as a function of $\omega_{\rm lab}$. The analyzing powers A_y are significantly smaller than the induced polarization P at all three angles in the whole energy transfer region. The values of A_y decrease with increasing $\omega_{\rm lab}$ beyond the quasielastic peak, whereas the values of P are always larger than 0.15. The solid and dashed curves represent the DWIA + RPA results for A_y and P, respectively. The calculations give almost the same values of A_y and P over the whole region and agree reasonably well with the experimental A_y data around the quasielastic peak.

Similar differences between A_y and P are observed in the highest momentum transfer measurements reported for quasielastic (p,n) reactions at T_p = 197 MeV [35]. A possible origin of these differences might be off-energy-shell effects in the quasielastic scattering process. These effects can be represented in part by the D term in a Kerman-McManus-Thaler (KMT) [43] representation of the effective *NN t* matrix. The quantity $(P-A_y)$ of the *NN* scattering is given in PWIA by

$$P - A_y = \frac{\mathrm{Im}[(E-F)D^*]}{I_0}, \tag{1}$$

where E and F are spin-dependent KMT amplitudes and I_0 is the cross section. Note that this quantity is zero in free *NN* scattering where $D=0$. Noro *et al.* [44] reported the measurement of polarization observables for proton knockout $(p,2p)$ reactions from $s_{1/2}$ orbits of nuclear targets with T_p = 392 MeV polarized protons. The *NN* amplitudes determined from their data suggest a significant D value, which corresponds to their positive $(P-A_y)$ values. We could not use the $(p,2p)$ result directly for interpretation of our (p,n) data because not only are the momentum and energy transfers different but the relevant isospin is different also. Nevertheless the plausible contribution of the D term might be responsible for $(P-A_y)\neq 0$ in quasielastic (p,n) reactions.

Figure 3 compares the polarization transfer coefficients D_{ij} for ^{12}C$(\vec{p},\vec{n})$ at $\theta_{\rm lab}$ = 16°, 22°, and 27° with the DWIA calculations. The data at $\theta_{\rm lab}$ = 22° were taken from our previous paper [34]. The solid curves represent the DWIA

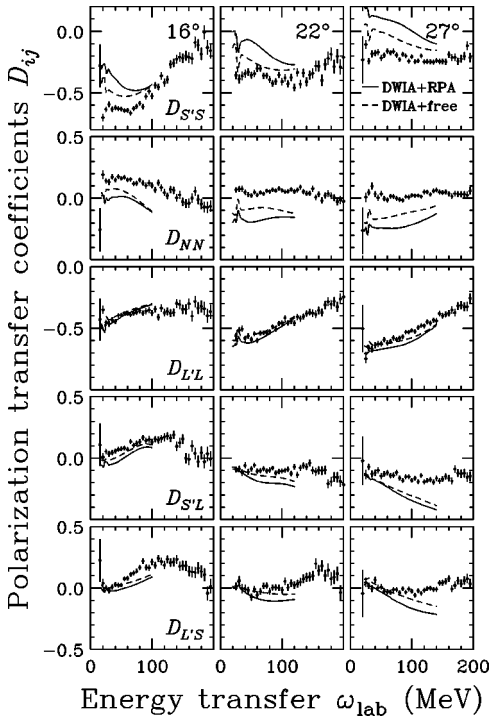

FIG. 3. Polarization transfer coefficients for the ^{12}C(p,n) reaction at T_p=345 MeV and $\theta_{\rm lab}$=16°, 22°, and 27°. The data are binned in 5-MeV steps. The solid and dashed curves denote the DWIA+RPA and DWIA+free results, respectively.

+RPA results, and the dashed curves are the results of the DWIA calculations with the free response functions designated herein as DWIA+free. The effects of the RPA correlations are significantly larger for $D_{S'S}$ and D_{NN} than they are for other D_{ij}'s. For $D_{S'S}$ and D_{NN}, the results with the free response functions are closer to the experimental data than those with the RPA correlations. For other D_{ij}'s, both calculations with and without the RPA correlations reproduce the experimental data reasonably well.

IV. METHOD OF ANALYSIS

In this section, we compare the experimental polarized cross sections with the DWIA+RPA calculations in order to investigate the nuclear correlation effects.

TABLE I. Meson parameters used in the present calculations [46]. Nucleon and Δ-isobar masses are 939 MeV and 1232 MeV, respectively. The ratio of the $N\Delta$ coupling to the NN one is $f_{\pi N\Delta}/f_{\pi NN}=f_{\rho N\Delta}/f_{\rho NN}=\sqrt{72/25}=1.70$. The ratio of the rho-meson coupling to the pion one is $C_\rho\equiv[(f_{\rho NN}/f_{\pi NN})(m_\pi/m_\rho)]^2=[(f_{\rho N\Delta}/f_{\pi N\Delta})(m_\pi/m_\rho)]^2=2.94$.

Vertex α	m_α (MeV)	f_α	Λ_α (MeV)	n_α
πNN	138	0.99	1300	1
$\pi N\Delta$	138	1.68	1200	1
ρNN	769	9.45	1400	1
$\rho N\Delta$	769	16.03	1400	2

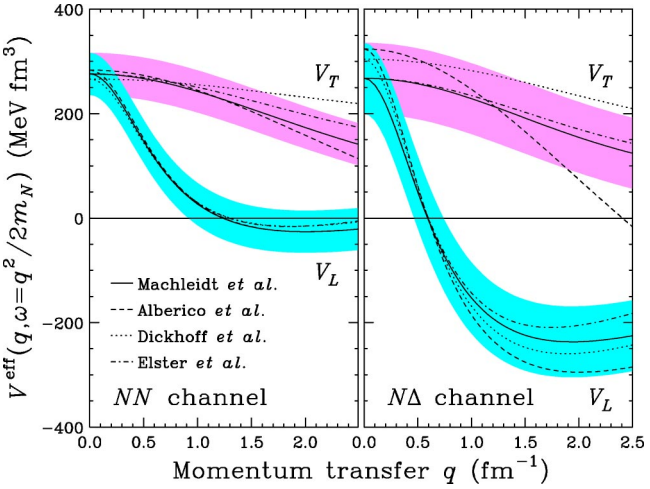

FIG. 4. (Color online) Momentum transfer dependence of the spin-londitudinal and spin-transverse effective interactions, V_L and V_T, in the NN (left panel) and $N\Delta$ (right panel) channels. The solid curves are the results with the meson parameters used by Machleidt *et al.* [46] employing $(g'_{NN},g'_{N\Delta})=(0.7,0.4)$. The bands represent the g'_{NN} and $g'_{N\Delta}$ dependences of the effective interactions within $0.6\leqslant g'_{NN}\leqslant 0.8$ (NN channel) and $0.3\leqslant g'_{N\Delta}\leqslant 0.5$ ($N\Delta$ channel). The dashed, dotted, and dot-dashed curves denote the results with the meson parameters used by Alberico *et al.* [1], Dickhoff *et al.* [62], and Elster *et al.* [63], respectively. The Landau-Migdal parameters are set to $(g'_{NN},g'_{N\Delta})=(0.7,0.4)$.

A. Coordinate system

The momentum transfer of the center-of-mass (c.m.) system is given by

$$\mathbf{q}=\mathbf{k}'-\mathbf{k}, \tag{2}$$

where $\mathbf{k}$ and $\mathbf{k}'$ are the momenta of the incident and outgoing nucleons in the c.m. frame, respectively. We use the c.m. coordinate system (q,n,p) defined as

$$\hat{\mathbf{q}}=\frac{\mathbf{q}}{|\mathbf{q}|}, \tag{3a}$$

$$\hat{\mathbf{n}}=\frac{\mathbf{k}\times\mathbf{k}'}{|\mathbf{k}\times\mathbf{k}'|}, \tag{3b}$$

$$\hat{\mathbf{p}}=\hat{\mathbf{q}}\times\hat{\mathbf{n}}. \tag{3c}$$

B. Polarized cross sections

The unpolarized double differential cross section I ($\sigma_{\rm lab}$ in Fig. 1) in the laboratory frame is decomposed into the four polarized cross sections ID_i as

$$I=ID_0+ID_q+ID_n+ID_p, \tag{4}$$

where D_i are the polarization observables introduced by Bleszynski *et al.* [45], and they are related to D_{ij} in the laboratory frame as [23]

$$D_0 = \frac{1}{4}[1 + D_{NN} + (D_{S'S} + D_{L'L})\cos\ \alpha_1 + (D_{L'S} - D_{S'L})\sin\ \alpha_1], \tag{5a}$$

$$D_n = \frac{1}{4}[1 + D_{NN} - (D_{S'S} + D_{L'L})\cos\ \alpha_1 - (D_{L'S} - D_{S'L})\sin\ \alpha_1], \tag{5b}$$

$$D_q = \frac{1}{4}[1 - D_{NN} + (D_{S'S} - D_{L'L})\cos\ \alpha_2 - (D_{L'S} + D_{S'L})\sin\ \alpha_2], \tag{5c}$$

$$D_p = \frac{1}{4}[1 - D_{NN} - (D_{S'S} - D_{L'L})\cos\ \alpha_2 + (D_{L'S} + D_{S'L})\sin\ \alpha_2], \tag{5d}$$

where $\alpha_1 \equiv \theta_{\rm lab} + \Omega$ and $\alpha_2 \equiv 2\theta_p - \theta_{\rm lab} - \Omega$. The angle θ_p represents the angle between $\hat{\mathbf{k}}$ and $\hat{\mathbf{p}}$, and Ω is the the relativistic spin rotation angle defined in Ref. [23].

C. RPA formalism

The RPA formalism is that of Nishida and Ichimura [12] and Kawahigashi *et al.* [38], and the spin response functions are calculated via the continuum RPA with the ring approximation including the Δ degrees of freedom. The RPA correlations are taken into account only in the isovector spin-dependent modes. For the effective interaction in these modes, we employ the $(\pi+\rho+g')$ model, in which it is written as

$$V^{\rm eff}(\mathbf{q},\omega) = V_L^{\rm eff}(\mathbf{q},\omega) + V_T^{\rm eff}(\mathbf{q},\omega), \tag{6}$$

where $V_L^{\rm eff}$ and $V_T^{\rm eff}$ are spin-longitudinal and spin-transverse effective interactions, respectively. They are given by

$$V_L^{\rm eff}(\mathbf{q},\omega) = \left[\frac{f_{\pi NN}^2}{m_\pi^2}\left(g'_{NN} + \Gamma_{\pi NN}^2(q,\omega)\frac{q^2}{\omega^2 - q^2 - m_\pi^2}\right)(\sigma_1\cdot\hat{\mathbf{q}})(\sigma_2\cdot\hat{\mathbf{q}})(\tau_1\cdot\tau_2) + \frac{f_{\pi NN}f_{\pi N\Delta}}{m_\pi^2}\left(g'_{N\Delta} + \Gamma_{\pi NN}(q,\omega)\Gamma_{\pi N\Delta}(q,\omega)\frac{q^2}{\omega^2 - q^2 - m_\pi^2}\right)\{(\sigma_1\cdot\hat{\mathbf{q}})(\mathbf{S}_2\cdot\hat{\mathbf{q}})(\tau_1\cdot\mathbf{T}_2) + (1\leftrightarrow 2)\} + \frac{f_{\pi N\Delta}^2}{m_\pi^2}\left(g'_{\Delta\Delta} + \Gamma_{\pi N\Delta}^2(q,\omega)\frac{q^2}{\omega^2 - q^2 - m_\pi^2}\right)(\mathbf{S}_1\cdot\hat{\mathbf{q}})(\mathbf{S}_2\cdot\hat{\mathbf{q}})(\mathbf{T}_1\cdot\mathbf{T}_2)\right] \tag{7}$$

and

$$V_T^{\rm eff}(\mathbf{q},\omega) = \left[\frac{f_{\pi NN}^2}{m_\pi^2}\left(g'_{NN} + C_\rho\Gamma_{\rho NN}^2(q,\omega)\frac{q^2}{\omega^2 - q^2 - m_\rho^2}\right)(\sigma_1\times\hat{\mathbf{q}})(\sigma_2\times\hat{\mathbf{q}})(\tau_1\cdot\tau_2) + \frac{f_{\pi NN}f_{\pi N\Delta}}{m_\pi^2}\left(g'_{N\Delta} + C_\rho\Gamma_{\rho NN}(q,\omega)\Gamma_{\rho N\Delta}(q,\omega)\frac{q^2}{\omega^2 - q^2 - m_\rho^2}\right)\{(\sigma_1\times\hat{\mathbf{q}})(\mathbf{S}_2\times\hat{\mathbf{q}})(\tau_1\cdot\mathbf{T}_2) + (1\leftrightarrow 2)\} + \frac{f_{\pi N\Delta}^2}{m_\pi^2}\left(g'_{\Delta\Delta} + C_\rho\Gamma_{\rho N\Delta}^2(q,\omega)\frac{q^2}{\omega^2 - q^2 - m_\rho^2}\right)(\mathbf{S}_1\times\hat{\mathbf{q}})(\mathbf{S}_2\times\hat{\mathbf{q}})(\mathbf{T}_1\cdot\mathbf{T}_2)\right], \tag{8}$$

where m_π and m_ρ are the pion and rho-meson masses, σ and τ are the spin and isospin operators of the nucleon N, and $\mathbf{S}$ and $\mathbf{T}$ are the spin and isospin transition operators from N to Δ. The constants $f_{\pi NN}$, $f_{\pi N\Delta}$, $f_{\rho NN}$, and $f_{\rho N\Delta}$ are the πNN, $\pi N\Delta$, ρNN, and $\rho N\Delta$ coupling constants, respectively. The Landau-Migdal parameters, g'_{NN}, $g'_{N\Delta}$, and $g'_{\Delta\Delta}$, correspond to the NN, $N\Delta$, and $\Delta\Delta$ channels, respectively. The coefficient C_ρ is the ratio of the rho-meson coupling to the pion one. The vertex form factors, Γ_α ($\alpha = \pi NN$, $\pi N\Delta$, ρNN or $\rho N\Delta$), are parametrized in the conventional form of

$$\Gamma_\alpha = \left(\frac{m_\alpha^2 - \Lambda_\alpha^2}{\omega^2 - q^2 - \Lambda_\alpha^2}\right)^{n_\alpha}, \tag{9}$$

where Λ_α are the cutoff parameters, $n_\alpha = 1$ (monopole) or 2 (dipole) depending on the specific coupling, $m_{\pi NN} = m_{\pi N\Delta} = m_\pi$, and $m_{\rho NN} = m_{\rho N\Delta} = m_\rho$.

Table I summarizes the herein used meson parameters from a Bonn potential which treats Δ explicitly [46]. In Fig. 4, the resulting V_L and V_T at $\omega = q^2/(2m_N)$ in the NN and $N\Delta$

channels are shown by the solid curves. The Landau-Migdal parameters of $(g'_{NN}, g'_{N\Delta}) = (0.7, 0.4)$ are adjusted to reproduce the experimental ID_q.

The mean field for the single-particle wave functions is given by

$$U(r) = -(V_0 + iW_0) f_{\rm WS}(r) + \frac{2}{m_\pi^2} V_{ls} \frac{d}{dr} f_{\rm WS}(r) \mathbf{l} \cdot \mathbf{s} + V_C(r), \tag{10}$$

where $V_C(r)$ is the Coulomb potential, $f_{\rm WS}(r)$ is the Woods-Saxon radial form factor with the radial parameter $r_0 = 1.27$ fm and the diffuseness $a = 0.67$ fm. The spin-orbit potential V_{ls} is chosen to be 6.5 MeV and 10.0 MeV for ^{12}C and ^{40}Ca, respectively. The real potential V_0 is determined to reproduce the observed separation energy of the outermost occupied state of the target nucleus. The imaginary potential W_0 is obtained by using the empirical formula for the spreading width [47,48]. For the Δ isobar, we set $V_0 = 30$ MeV and $W_0 = V_{ls} = 0$ MeV.

The nonlocality of the mean field is simulated by the radial-dependent effective mass

$$m^*(r) = m_N - \frac{f_{\rm WS}(r)}{f_{\rm WS}(0)} [m_N - m^*(0)], \tag{11}$$

with $m^*(0) = 0.7 m_N$. Effects of m^* are easily estimated by the Fermi gas model in which the quasielastic distribution peaks at $q^2/2m^*$ and its height and width are given by $3m^*/4qp_F$ and qp_F/m^*, respectively, where p_F is the Fermi momentum. The parameters of $U(r)$ and $m^*(r)$ are the same as used in Ref. [38].

D. DWIA formalism

We use the formalism given by Kawahigashi *et al.* [38] for the DWIA calculations. The distorted waves for incident and outgoing particles are calculated by using global optical potentials based on Dirac phenomenology [49]. The optimal factorization prescription [20–23] is employed to model the Fermi motion of the target nucleons. The free *NN t*-matrix parameters are taken from those of Bugg and Wilkin [50].

V. COMPARISON TO DWIA+RPA CALCULATIONS

A. RPA effects

Figure 5 compares the experimental polarized cross sections ID_q and ID_p with the DWIA calculations. The dashed curves are the results of DWIA with the free response functions employing $m^*(0) = 0.7 m_N$. Both of the experimental ID_q and ID_p are significantly larger than those predicted via the DWIA+free calculations. The solid curves denote the results of the DWIA+RPA calculations with the RPA parameters of $(g'_{NN}, g'_{N\Delta}) = (0.7, 0.4)$ and $m^*(0) = 0.7 m_N$. Since both the spin-longitudinal and spin-transverse polarized cross sections, ID_q and ID_p, are insensitive to the $g'_{\Delta\Delta}$ parameter [12], it was arbitrarily set at $g'_{\Delta\Delta} = 0.5$ [51].

For the spin-longitudinal mode, the DWIA+RPA calculations at $\theta_{\rm lab} = 22°$ and 27° reproduce the experimental data

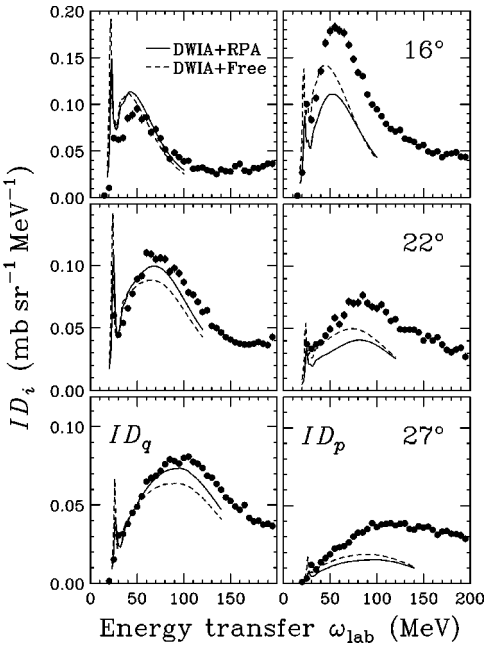

FIG. 5. The spin-longitudinal (left panels) and spin-transverse (right panels) polarized cross sections, ID_q and ID_p, for the ^{12}C(p,n) reaction at $T_p = 345$ MeV and $\theta_{\rm lab} = 16°$, 22°, and 27°. The solid curves represent the DWIA calculations employing the RPA response functions with $(g'_{NN}, g'_{N\Delta}) = (0.7, 0.4)$ and $m^*(0) = 0.7 m_N$. The dashed curves are the DWIA+free results with $m^*(0) = 0.7 m_N$.

reasonably well below the quasielastic peak, whereas they slightly underestimate the data beyond the quasielastic peak where two-step contributions should be important, as is shown in Sec. VI. The calculations at $\theta_{\rm lab} = 16°$ significantly overestimate the data below the quasielastic peak. The quasielastic peak of ID_q in the DWIA+RPA calculations corresponds to the excitation energy of $E_x \simeq 22$ MeV at $\theta_{\rm lab} = 16°$. In the low lying states of ^{12}C and ^{12}N, it is well known that there are strong nuclear correlations beyond RPA in the mean field theory. The contributuons from these states decreases relative to those from the quasielastic process with increasing reaction angle. We will see in Sec. VI that the RPA correlations in the spin-longitudinal mode explain the experimentally observed enhancement in ID_q at large angles when two-step contributions are included.

The g'_{NN} and $g'_{N\Delta}$ dependences of the DWIA+RPA calculations are investigated in Fig. 6. We show only the results at $\theta_{\rm lab} = 22°$ since the results at other angles are very similar. The upper panels of Fig. 6 represent the g'_{NN} dependence in $0.6 \leqslant g'_{NN} \leqslant 0.8$ with the fixed $g'_{N\Delta} = 0.4$. The solid curves are the results with $g'_{NN} = 0.7$. The upper boundaries of the bands correspond to the results with $g'_{NN} = 0.6$, whereas the lower ones are the results with $g'_{NN} = 0.8$. The g'_{NN} dependence is observed for ID_q near and below the quasielastic peak. The experimental data are best fitted with a large g'_{NN} value below the quasielastic peak and a smaller g'_{NN} value around the peak. We should note that it is not appropriate to determine g'_{NN} from low energy transfers where there appear strong nuclear correlations beyond RPA.

The middle panels of Fig. 6 show the $g'_{N\Delta}$ dependence of the DWIA+RPA calculations in $0.3 \leqslant g'_{N\Delta} \leqslant 0.5$ with the

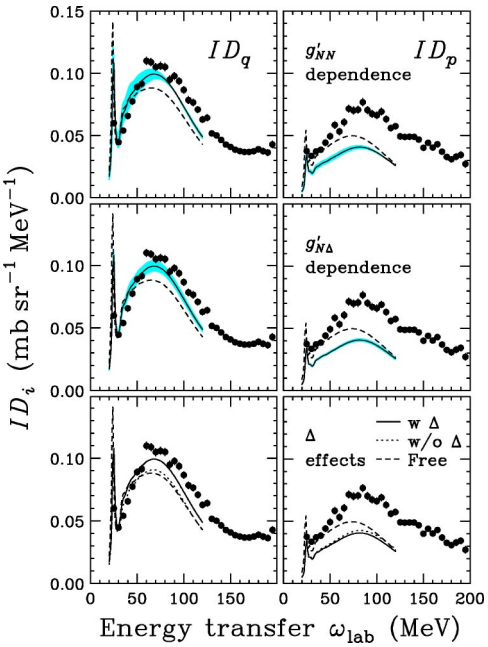

FIG. 6. (Color online) Measurements of the polarized cross sections for the ^{12}C(p,n) reaction at T_p=345 MeV and θ_{lab}=22°. The solid and dashed curve are the same as those in Fig. 5. The bands show the g'_{NN} (top panels) and $g'_{N\Delta}$ (middle panels) dependences of the DWIA+RPA calculations. The dotted curves in the bottom panels represent the DWIA+RPA results without Δ.

fixed g'_{NN}=0.7. The upper and lower boundaries of the bands correspond to the results with $g'_{N\Delta}$=0.3 and 0.5, respectively. The solid curves are the results with $g'_{N\Delta}$=0.4. The $g'_{N\Delta}$ dependence is clearly observed for ID_q around the quasielastic peak. The experimental data are best fitted with a small $g'_{N\Delta}$ value. However, the optimal g'_{NN} and $g'_{N\Delta}$ may not be found without taking multistep contributions into account, as will be discussed in Sec. VI.

For the spin-transverse mode, the results of the same calculations are shown in the right panels of Figs. 5 and 6. The reduction from the dashed curves to the solid ones elucidates the quenching of ID_p as predicted, while the experimental data are enhanced. The g'_{NN} and $g'_{N\Delta}$ dependences shown by the bands are small for ID_p, as predicted in Ref. [12]. The observed ID_p data are much larger than the calculations, and inclusion of two-step contributions is required in order to resolve this discrepancy.

B. Δ Effects

The lower panels of Fig. 6 show the Δ effects in the DWIA+RPA calculations. The solid and dotted curves represent the DWIA calculations employing the RPA response functions with and without Δ, respectively. The dashed curves are the results with the free response functions. The Landau-Migdal parameters g'_{NN} and $g'_{N\Delta}$ are set equal to 0.7 and 0.4, respectively, while the other parameters were left unchanged.

The spin-longitudinal effective interaction in the *NN* channel is given by the first term of Eq. (7). Since its magnitude is very small, as seen by the solid curves of Fig. 4, the RPA results without Δ are close to the free ones. Once Δ is introduced, ID_q is enhanced in the whole quasielastic region, as seen in Fig. 6. The enhancement is attributed to the attractive effective interaction in the $N\Delta$ channel given by the second term of Eq. (7). This interaction brings the spin-longitudinal strength down from the Δ-hole sector to the particle-hole one, and thus the Δ plays an essential role in the enhancement of the spin-longitudinal mode.

In the spin-transverse mode, the RPA results with and without Δ are very close to each other. The spin-transverse part of the effective interaction in the $N\Delta$ channel given by the second term of Eq. (8) is relatively small compared to the spin-longitudinal part [12] (see the solid curves of Fig. 4). Thus the Δ effects for ID_p are considerably smaller than those for ID_q.

VI. TWO-STEP CONTRIBUTIONS

The abnormally large ID_p relative to the theoretical predictions may be due to the absence of some reaction mechanisms such as two-step processes in the DWIA calculations.

In the two-step calculation, the motion of the scattering nucleon (the incident proton, the nucleon in intermediate states, and the outgoing neutron) is treated as the plane wave (PWA). We assume that the scattering nucleons in the one- and two-step processes follow similar trajectories, and therefore nuclear distortion and absorption effects for two-step processes are similar to those for the one-step process. Hence we estimate the effects by the ratio of DWIA to PWIA cross sections for the one-step process. Then the two-step contribution with these effects is given by

$$\text{2-step with distortion effects} \simeq \text{2-step in PWA} \times \frac{\text{DWIA}}{\text{PWIA}}. \tag{12}$$

In the present two-step calculation, a target is treated as a simple double closed-shell state. Thus DWIA and PWIA calculations in Eq. (12) are also performed with the free response functions.

Figure 7 compares experimental ID_q and ID_p for ^{12}C with theoretical calculations that include both the DWIA+RPA results as well as two-step contributions. In Fig. 8 we also compare the experimental and theoretical results for the ^{40}Ca(p,n) reaction at θ_{lab}=22°. To evaluate the experimental ID_i for ^{40}Ca, the unpolarized cross section I measured in the present experiment is used, while the D_i values are from previous work [34]. Thus the ID_i values in Fig. 8 are smaller than those in Ref. [34] by a factor of about 0.82, as discussed in Ref. [42].

The one-step DWIA calculations with the RPA and free response functions are shown as the thin-solid and dashed curves, respectively. The dotted curves represent the two-step contributions defined in Eq. (12). The thick-solid curves are the sums of one-step of DWIA+RPA and two-step contributions. The RPA uses the same Landau-Migdal parameters used in the calculations in Fig. 5.

For ID_q, the RPA correlations enhance the results of the calculations from the dashed to thin-solid curves, and the

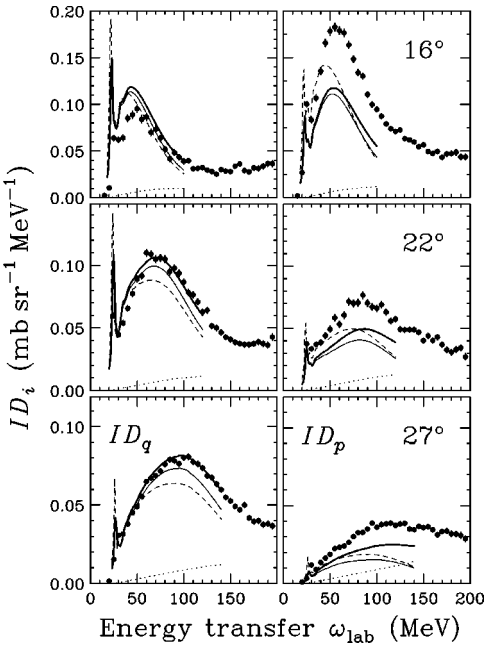

FIG. 7. The two-step contributions (dotted curves) in ID_q (left panels) and ID_p (right panels) for the ^{12}C(p,n) reaction at T_p =345 MeV and $\theta_{\rm lab}$=16°, 22°, and 27°. The thick-solid curves denote the sums of the DWIA+RPA and the two-step contributions. The solid and dashed curve are the same as those in Fig. 5.

two-step contributions increase the results from the thin-solid to thick-solid curves. We can see that both the pionic enhancement in RPA and the two-step contributions play important roles in explaining the experimental data near and beyond the quasielastic peak. The discrepancy between the experimental and theoretical results at $\theta_{\rm lab}$=16° in low energy transfers below the quasielastic peak might be due to the nuclear correlations beyond RPA, as discussed in Sec. V. Although calculations are not sensitive to Landau-Migdal parameters, as shown by the bands in Fig. 6, the best values are $g'_{NN}=0.7\pm0.1$ and $g'_{N\Delta}=0.4\pm0.1$, which are somewhat larger than those obtained without two-step contributions [38], and are consistent with those evaluated from the quenching factor of the Gamow-Teller sum rule [52] taking into account finite nuclear effects [53].

The RPA correlations induced by the spin-transverse interaction $(\rho+g')$ quench the spin-transverse response function R_T and its relevant polarized cross section ID_p. However, the experimental results are much larger than the DWIA calculation with the RPA correlation. The relative importance of two-step contributions for ID_p is significantly larger than that for ID_q [54,55]. They account for the underestimation of ID_p in the DWIA+RPA calculation at large energy transfers beyond the quasielastic peak. However, these effects are not sufficient to explain the underestimation of ID_p. This discrepancy might be due to the effects of the higher-order (such as 2p2h) configuration mixing [56–60] and/or the medium modifications of the effective *NN* interaction. A sizable modification has been suggested from the study of the proton inelastic scattering on ^{28}Si to the stretched 6^-, $T=1$ state at 14.36 MeV with T_p=198 MeV polarized protons [61]. We could not use this result for interpretation of the discrepancy because of the different reaction and the different energy. Thus we need further theoretical and experimental studies in order to settle the discrepancy.

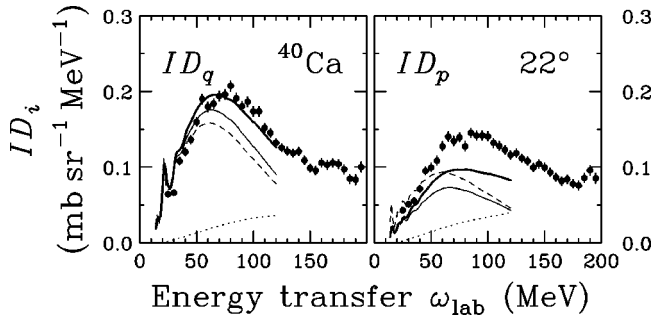

FIG. 8. Same as Fig. 7 but for the ^{40}Ca(p,n) reaction at T_p =346 MeV and $\theta_{\rm lab}$=22°.

VII. FINAL REMARKS

The g' values and thus the effective interactions in Eqs. (7) and (8) depend upon the choice of meson parameters. The bands in Fig. 4 show the g'_{NN} and $g'_{N\Delta}$ dependence of the effective interactions. The upper and lower boundaries in the *NN* channel correspond to the results with g'_{NN}=0.8 and 0.6, respectively, whereas those in the $N\Delta$ channel represent the results with $g'_{N\Delta}$=0.5 and 0.3, respectively. Since the present ID_p data are insensitive to the spin-transverse interactions, as discussed in Sec. V, only the spin-longitudinal interactions will be discussed below.

Although the spin-longitudinal interactions in the *NN* channel are close to zero in the momentum-transfer region of $q=1.2-2.0$ fm^{-1}, those in the $N\Delta$ channel are very attractive in the same region. This attraction causes the enhancement of the spin-longitudinal mode.

The dashed, dotted, and dot-dashed curves in Fig. 4 are the results employing the same values of $(g'_{NN},g'_{N\Delta})$ $=(0.7,0.4)$ but with other meson parameters used by Alberico *et al.* [1], Dickhoff *et al.* [62], and Elster *et al.* [63], respectively. The results in the *NN* channel are almost independent of the choice of meson parameters. However, those in the $N\Delta$ channel change their values within the band. For example, in the present momentum-transfer region, the result with the parameters used by Alberico *et al.* [1] becomes more attractive than the present result shown by the solid curve. This means that their meson parameters prefer a larger $g'_{N\Delta}$ value of $\simeq$0.5. On the contrary, the meson parameters used by Elster *et al.* [63] favor a smaller $g'_{N\Delta}$ value. Therefore, it is important to discuss the Landau-Migdal parameters and the meson parameters simultaneously in the analysis of finite q since the effective interactions are the functions of both.

VIII. SUMMARY AND CONCLUSION

The cross sections, analyzing powers, induced polarizations, and a complete set of polarization transfer coefficients for quasielastic $(\vec{p},\vec{n})$ reactions on ^{12}C and ^{40}Ca were measured at T_p=345 MeV. The reaction angles are $\theta_{\rm lab}$=16°,

22°, and 27° for ^{12}C and $\theta_{\rm lab}=22°$ for ^{40}Ca, which corresponds to the laboratory momentum transfers of $q_{\rm lab} \simeq 1.2-2.0$ fm^{-1} where the effective interaction in the one-pion exchange channel is attractive.

The experimental spin-longitudinal and spin-transverse polarized cross sections are compared with DWIA calculations employing the RPA response functions inclusive of two-step contributions. The enhancement of ID_q from the RPA correlations including Δ effects is important in explaining the experimental data. The comparison between the experimental and theoretical results supports the Landau-Migdal parameters of $g'_{NN}=0.7\pm0.1$ and $g'_{N\Delta}=0.4\pm0.1$. This means that the universality ansatz [3,4,64] of $g'_{NN}=g'_{N\Delta}=g'_{\Delta\Delta}=g'$ does not hold, and $g'_{N\Delta}$ is much smaller than g'_{NN} in the present momentum-transfer region. These values are consistent with those at $q=0$ obtained from the quenching factor of the Gamow-Teller sum rule.

The two-step contributions account for the underestimation of ID_q in the DWIA calculations with the RPA correlations at large energy transfers beyond the quasielastic peak. In the spin-transverse mode, the relative importance of two-step contributions is significantly larger than that for ID_q. However, they are insufficient to explain the underestimation of ID_p around the quasielastic peak.

The present analysis shows that the enhancement of the spin-longitudinal response function R_L and the relevant polarized cross section ID_q is supported by the experiment, which implies the appearence of the precursor phenomena of the pion condensation in the normal nuclei. However, the anomaly in the spin-transverse mode pointed out firstly by Taddeucci *et al.* [33] and also by Wakasa *et al.* [34] has been still unresolved. To understand the quantitative difference between the experimental and theoretical ID_p, we need further investigation on higher-order configuration mixing as well as additional theoretical and experimental studies of the effective *NN t*-matrix in nuclear medium.

ACKNOWLEDGMENTS

We thank Professor H. Toki for encouragement throughout the work, and the RCNP cyclotron crew for their efforts in providing a high quality polarized proton beam. The experiment was performed at RCNP under Program Number E131. This work was supported in part by the Grants-in-Aid for Scientific Research Nos. 12640294, 12740151, and 14702005 of the Ministry of Education, Culture, Sports, Science, and Technology of Japan.

[1] W. M. Alberico, M. Ericson, and A. Molinari, Nucl. Phys. **A379**, 429 (1982).
[2] M. Ericson and J. Delorme, Phys. Lett. **76B**, 182 (1978).
[3] H. Toki and W. Weise, Phys. Rev. Lett. **42**, 1034 (1979).
[4] W. M. Alberico, M. Ericson, and A. Molinari, Phys. Lett. **92B**, 153 (1980).
[5] H. Toki and W. Weise, Phys. Lett. **92B**, 265 (1980).
[6] C. H. L. Smith, Phys. Lett. **128B**, 107 (1983).
[7] M. Ericson and A. W. Thomas, Phys. Lett. **128B**, 112 (1983).
[8] B. L. Friman, V. R. Pandharipande, and R. B. Wiringa, Phys. Rev. Lett. **51**, 763 (1983).
[9] E. L. Berger, F. Coester, and R. B. Wiringa, Phys. Rev. D **29**, 398 (1984).
[10] D. Stump, G. F. Bertsch, and J. Pumlin, in *Hadron Substructure in Nuclear Physics*, edited by W-Y P. Hwang *et al.*, AIP Conf. Proc. 110 (AIP, New York, 1984), p. 339.
[11] D. S. Koltun, Phys. Rev. C **57**, 1210 (1998).
[12] K. Nishida and M. Ichimura, Phys. Rev. C **51**, 269 (1995).
[13] P. Barreau *et al.*, Nucl. Phys. **A402**, 1983 (1983).
[14] Z. E. Meziani *et al.*, Phys. Rev. Lett. **54**, 1233 (1985).
[15] A. Zghiche *et al.*, Nucl. Phys. **A572**, 513 (1994).
[16] M. Deady *et al.*, Phys. Rev. C **28**, 631 (1983).
[17] M. Deady, C. F. Williamson, P. D. Zimmerman, R. Altemus, and R. R. Whitney, Phys. Rev. C **33**, 1897 (1986).
[18] C. C. Blatchley, J. J. LeRose, O. E. Pruet, P. D. Zimmerman, C. F. Williamson, and M. Deady, Phys. Rev. C **34**, 1243 (1986).
[19] C. F. Williamson *et al.*, Phys. Rev. C **56**, 3152 (1997).
[20] A. Picklesimer, P. C. Tandy, R. M. Thaler, and D. H. Wolfe, Phys. Rev. C **30**, 1861 (1984).
[21] S. A. Guyrvitz, Phys. Rev. C **33**, 422 (1986).
[22] X. Q. Zhu, N. Mobed, and S. S. M. Wong, Nucl. Phys. **A466**, 623 (1987).
[23] M. Ichimura and K. Kawahigashi, Phys. Rev. C **45**, 1822 (1992).
[24] T. A. Carey, K. W. Jones, J. B. McClelland, J. M. Moss, L. B. Rees, N. Tanaka, and A. D. Bacher, Phys. Rev. Lett. **53**, 144 (1984).
[25] L. B. Rees, J. M. Moss, T. A. Carey, K. W. Jones, J. B. McClelland, N. Tanaka, A. D. Bacher, and H. Esbensen, Phys. Rev. C **34**, 1986 (1986).
[26] R. Fergerson, J. McGill, C. Glashausser, K. Jones, S. Nanda, S. Zuxun, M. Barlett, G. Hoffmanna, J. Marshall, and J. McClelland, Phys. Rev. C **38**, 1988 (1988).
[27] O. Häusser *et al.*, Phys. Rev. Lett. **61**, 822 (1988).
[28] C. Chan *et al.*, Nucl. Phys. **A510**, 713 (1990).
[29] W. M. Alberico, A. D. Pace, M. Ericson, M. B. Johnson, and A. Molinari, Phys. Rev. C **38**, 109 (1988).
[30] M. Ichimura, K. Kawahigashi, T. S. Jorgensen, and C. Gaarde, Phys. Rev. C **39**, 1446 (1989).
[31] J. B. McClelland *et al.*, Phys. Rev. Lett. **69**, 582 (1992).
[32] X. Y. Chen *et al.*, Phys. Rev. C **47**, 2159 (1993).
[33] T. N. Taddeucci *et al.*, Phys. Rev. Lett. **73**, 3516 (1994).
[34] T. Wakasa *et al.*, Phys. Rev. C **59**, 3177 (1999).
[35] C. Hautala *et al.*, Phys. Rev. C **65**, 034612 (2002).
[36] G. F. Bertsch, L. Frankfurt, and M. Strikman, Science **259**, 773 (1993).
[37] G. E. Brown, M. Buballa, Z. B. Li, and J. Wambach, Nucl. Phys. **A593**, 295 (1995).
[38] K. Kawahigashi, K. Nishida, A. Itabashi, and M. Ichimura, Phys. Rev. C **63**, 044609 (2001).
[39] H. Sakai, H. Okamura, H. Otsu, T. Wakasa, S. Ishida, N. Saka-

moto, T. Uesaka, Y. Satou, S. Fujita, and K. Hatanaka, Nucl. Instrum. Methods Phys. Res. A **369**, 120 (1996).
[40] H. Sakai, H. Okamura, S. Ishida, K. Hatanaka, and T. Noro, Nucl. Instrum. Methods Phys. Res. A **320**, 479 (1992).
[41] T. Wakasa *et al.*, Nucl. Instrum. Methods Phys. Res. A **404**, 355 (1998).
[42] T. Wakasa *et al.*, Phys. Rev. C **69**, 044602 (2004).
[43] A. K. Kerman, H. MaManus, and R. M. Thaler, Ann. Phys. (N.Y.) **8**, 551 (1959).
[44] T. Noro *et al.*, in *Proceedings of the International Symposium on New Facet of Spin Giant Resonances in Nuclei, Tokyo, Japan, 1997*, edited by H. Sakai, H. Okamura, and T. Wakasa (World Scientific, Singapore, 1998), p. 378.
[45] E. Bleszynski, M. Bleszynski, and J. C. A. Whitten, Phys. Rev. C **26**, 2063 (1982).
[46] R. Machleidt, K. Holinde, and C. Elster, Phys. Rep. **149**, 1 (1987).
[47] C. Mahaux and N. Ngô, Phys. Lett. **100B**, 285 (1981).
[48] R. D. Smith and J. Wambach, Phys. Rev. C **38**, 100 (1988).
[49] E. D. Cooper, S. Hama, B. C. Clark, and R. L. Mercer, Phys. Rev. C **47**, 297 (1993).
[50] D. V. Bugg and C. Wilkin, Phys. Lett. **152B**, 37 (1985).
[51] J. M. ter Vehn, Phys. Rep. **74**, 323 (1981).
[52] T. Suzuki and H. Sakai, Phys. Lett. B **455**, 25 (1999).
[53] A. Arima, W. Bentz, T. Suzuki, and T. Suzuki, Phys. Lett. B **499**, 104 (2001).
[54] Y. Nakaoka and M. Ichimura, Prog. Theor. Phys. **102**, 599 (1999).
[55] Y. Nakaoka, Phys. Rev. C **65**, 064616 (2002).
[56] W. M. Alberico, M. Ericson, and A. Molinari, Ann. Phys. (N.Y.) **154**, 356 (1984).
[57] T. Suzuki, Nucl. Phys. **A495**, 581 (1989).
[58] K. Takayanagi, Nucl. Phys. **A516**, 276 (1990).
[59] J. Carlson and R. Schiavilla, Phys. Rev. C **49**, R2880 (1994).
[60] J. P. Adams and B. Castel, Phys. Rev. C **50**, R1763 (1994).
[61] E. J. Stephenson, J. Liu, A. Bacher, S. M. Bowyer, S. Chang, C. Olmer, S. P. Wells, and S. W. Wissink, Phys. Rev. Lett. **78**, 1636 (1997).
[62] W. H. Dickhoff, A. Faessler, J. M. ter Vehn, and H. Müther, Phys. Rev. C **23**, 1154 (1981).
[63] C. Elster, K. Holinde, D. Schütte, and R. Machleidt, Phys. Rev. C **38**, 1828 (1988).
[64] A. Bohr and B. R. Mottelson, Phys. Lett. **100B**, 10 (1981).